RESEARCH PAPER

Grafting of Ag Nanoparticles on SrMnO$_3$: Effect of Capping Agent and Alkaline Agent on the Morphology of SrMnO$_3$ Nanostructures for Enhancing Photocatalytic Performance

Mazyar Ahmadi Golsefidi[1],*, Hossein Khojasteh[2],*, Chalak Azimi[3], Ali Abbasi[1],*

[1] *Department of chemistry, Faculty of sciences, Gorgan branch, Islamic Azad University Gorgan, Iran*

[2] *Department of chemistry, Faculty of sciences, Soran University, PO Box 624, Soran, Kurdistan Regional Government, Iraq*

[3] *Department of chemistry, Faculty of sciences, Mahabad branch, Islamic Azad University, Mahabad, Iran*

ARTICLE INFO

ABSTRACT

In this work, SrMnO$_3$ nanoparticles were successfully synthesized using dimethylglyoxime (DMG) and triethylenepantamine (TEPA) as capping agent and alkaline agent respectively. To achieve the desired sample with high homogeneity and the fine size, various parameters such as capping agent, alkaline agent and temperature of calcination were changed. SrMnO$_3$ nanostructures with different morphologies such as unique sphere-like and hierarchical were successfully prepared. Then on the surface of the optimum sample, silver nanoparticles were doped. The as-synthesized nanostructures were characterized by thermal gravimetric analysis (TGA), X-ray diffraction (XRD), transmission electron microscopy (TEM), field emission scanning electron microscopy (FESEM), Fourier transform infrared (FT-IR) spectroscopy, energy dispersive X-ray microanalysis (EDX) and UV–Vis diffuse reflectance analysis (DRS). The photocatalytic degradation of the rhodamine B, methyl orange, murexide and methylene blue as water pollutants were investigated. According to the results, photocatalytic activity of SrMnO$_3$/Ag nanostructures were better and degradation percent of rhodamine B as a cationic pollutant was more than the other dyes.

How to cite this article
Ahmadi Golsefidi M., Khojasteh H., Azimi Gh., Abbasi A. Grafting of Ag Nanoparticles on SrMnO$_3$: Effect of Capping Agent and Alkaline Agent on the Morphology of SrMnO$_3$ Nanostructures for Enhancing Photocatalytic Performance. J Nanostruct, 2020; 10(4): 825-837. DOI: 10.22052/JNS.2020.04.016

INTRODUCTION

Newly, water cleaning is chosen as a serious challenge, therefore is known as one of the most significant fields in scientific research and organic dyes are the major pollutant types of wastewater. Up to now, numerous attempts has been dedicated to decline or demolition of pollutants in the wastewater. Of all the offers, photocatalyst way is known as one of the best and most promising routes for deletion organic contaminants from water [1-5]. In these processes, organic molecules decompose by interacting with a photo-catalyst material and UV or visible light and finally CO$_2$ and H$_2$O are achieved [6-9].

Different compounds of manganese used in various fields such as catalysis, batteries, photocatalysis, magnetite, and electrochemistry [10-12]. In recent years, many of the research groups studied the mixed-valent manganite AMnO$_3$ (A= Ca, Sr, Ba). The interesting properties of manganese oxides originated from the promise of technological applications [13]. Most of the studies

* Corresponding Author Email: ali.abbasi862@gmail.com

concentrated on the structures by $A_{1-x}R_xMnO_3$ formula. However, it found that a low number of works has been studied the $AMnO_3$ [14-16]. The $SrMnO_3$ is extensively used as antiferromagnetic insulator with a crystal structure of G-type [17, 18]. Due to the special skeletal structure which was consisted of a three dimensional network of MnO_6 octahedra, the $SrMnO_3$ sample has some properties such as oxygen nonstoichiometry, electronic properties, thermochromism, etc [19].

There are many methods for the synthesis of nanoparticles, including: sol-gel, hydrothermal, solvothermal method, reverse micelle methods, thermal decomposition, solid-state and sonochemical approach.

$SrMnO_3$ powders have been synthesized with many methods such as high temperature solid-state reaction, coprecipitation [20], sol-gel, etc [21-24]. High temperature solid-state reactions need a very high temperature. Furthermore, obtained products with this technique are agglomerated in a big grain size. Coprecipitation and sol-gel processes can prepare nanopowders in a lower temperature. Among the above methods for proportion particles in nanoscale, the co-precipitation approach is well-known as a high efficiency in the production of nanoparticles, simple process with high usability, cost-effective and production of high percent purity nanoparticles. Also this way is a very promising technique for the preparation of fine particles for mixed oxides, allowing controlled size and shape with commonly good combinatorial uniformly. In this work, we have reported the prepared of $SrMnO_3$ nanoparticles by co-precipitation process and then characterization by diverse techniques such as UV–Vis diffuse reflectance spectroscopy (DRS), energy dispersive X-ray microanalysis (EDX), Fourier transform infrared (FT-IR) spectroscopy, transmission electron microscopy (TEM), field emission scanning electron microscopy (FESEM) and X-ray diffraction (XRD). Then we examined the effects of various capping agents, alkaline agents and reaction temperature to achieve optimum conditions. Now the ability of $SrMnO_3$ as photocatalyst for the destruction of the organic dye including rhodamine B, methylene blue, murexide and methyl orange (as the model water pollutants) were studied. The effect of several factors such as type of pollutant, particle size and shape of $SrMnO_3$ nanostructures, pH and concentration of pollutant on photocatalytic behavior of products

was measured.

MATERIALS AND METHODS
Materials and Characterizations

Materials applied in this were Strontium nitrate ($Sr(NO_3)_2$, Merck, 99.9%), Manganese nitrate ($Mn(NO_3)_2$, Merck, 99.9%), $AgNO_3$, dimethylglyoxime (DMG), 2-hydroxy-1-naphthaldehyde, triethylenepantamine (abbreviated TEPA) and NH_3. All chemicals were used without further purification. Also de-ionized water was used as solvent. The XRD of products was recorded by Philips, X-ray diffractometer using Ni-filtered Cu Kα radiation. The EDX analysis with 20 kV accelerated voltage was done. FT Infrared (FT-IR) spectra were obtained as potassium bromide pellets in the range of 400–4000 cm^{-1} with a Nicolet-Impact 400D spectrophotometer. SEM images were taken using an LEO instrument model 1455VP. Prior to taking images, the samples were coated by a very thin layer of Pt (using a BAL-TEC SCD 005 sputter coater) to make the sample surface conductor, to prevent charge accumulation, and to obtain a better contrast. Transmission electron microscope (TEM) images of the as-obtained SrMnO3 nanostructures were taken on a JEM-2100 with an accelerating voltage of 200 kV. The UV–Vis diffuse reflectance spectrum of the as-produced $SrMnO_3$ nanostructures was obtained on a UV–Vis spectrophotometer (Shimadzu, UV-2550, Japan). Thermogravimetric analysis (TGA) was carried out using an instrument (Shimadzu TGA-50H) with a heating rate of 10 °C min-1 under nitrogen atmosphere.

Synthesis of $SrMnO_3$

The $SrMnO_3$ sample was synthesized using strontium nitrate, Manganese nitrate, TEPA and de-ionized water as solvents. In a typical method, 1 mmol of strontium nitrate and 1 mmol manganese nitrate individually dissolved in 20 ml of de-ionized water and then two solutions are mixed on magnetic stirrer at room temperature to achieve a homogeneous solution. Then 2 mmol of DMG, as a new capping agent, was added to the above solution and after it was stirred for 30 minutes. After 30 minutes stirring, triethylenepantamine as alkaline agent and capping agent was added dropwise into the mixed solution of Mn and Sr (pH= 10) and the temperature of the solution was maintained at about 70 °C. The formed precipitate was separated through centrifugation, washed by

Table 1. The reaction conditions for synthesis of SrMnO$_3$ via a precipitation method

| Sample No	Alkaline agent	Capping agent	Figure of SEM	Temperature of calcination	Ag-doped
1	NH$_3$	-	-	-	No
2	NH$_3$	-	5a and b	1000	No
3	TEPA	-	5c and d	1000	No
4	TEPA	2-hydroxy-1-naphthaldehyde	6a and b	1000	No
5	TEPA	DMG	6c and d	1000	No
6	TEPA	DMG	7a and b	1000	Yes
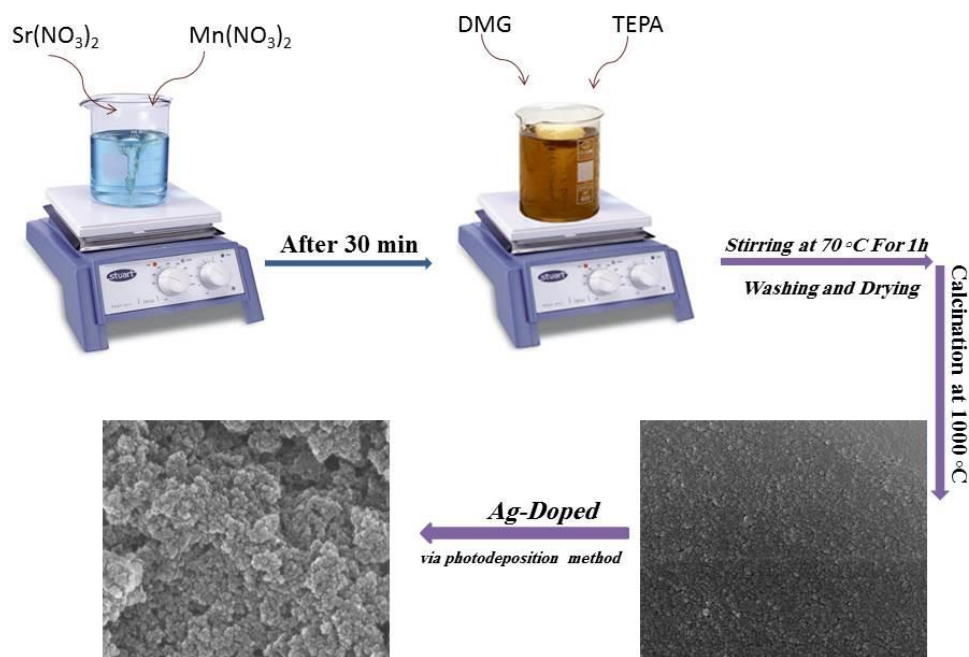
Fig. 1. Schematic diagram of the synthesis of SrMnO$_3$/Ag nanostructures

distilled water and ethanol, air-dried and at last calcined at 1000 °C for 5h. In Table 1 the production conditions of SrMnO$_3$ structures contain kind of capping agent and alkaline agent that effect on the shape, purity and grain size has been illustrated. For assessment the role of triethylenepantamine and DMG as a new precipitant and capping agent respectively, two samples were synthesized by NH$_3$ and 2-hydroxy-1-naphthaldehyde.

Synthesis of SrMnO$_3$/Ag nanocomposite

SrMnO$_3$/Ag nanoparticles were synthesized by photodeposition route. A suitable amount of AgNo$_3$ was dissolved in 25 ml deionized water and then 0.05 g SrMnO$_3$ was added to the above solution under magnetic stirring for 20 min. Next, 0.5 ml ethanol Merck added to solution. Deoxygenation

was also conducted simultaneously. Then the solution was transferred to quartz tube and stirred under UV irradiation for 3 hours. The formed product was separated and washed with deionized water and ethanol three times and dried at 70 °C Fig. 1.

Photocatalytic process

The photocatalytic activities of as-synthesized SrMnO$_3$ and SrMnO$_3$/Ag samples were done by monitoring the demolition of methylene blue, murexide, methyl orange and rhodamine B in aqueous solution, under irradiation with UV light. The maximum absorbance wavelength for rhodamine B, methylene blue, methyl orange and murexide are 543, 668, 510 and 506 nm respectively. The reaction mixture comprising of
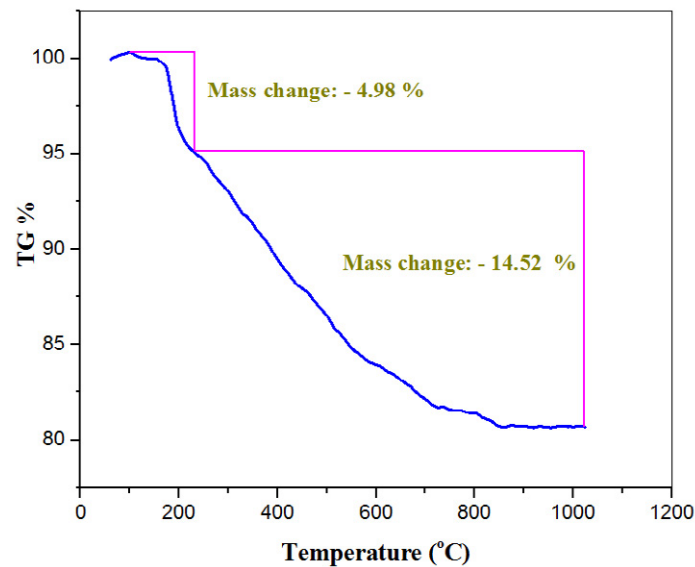
Fig. 2. TGA curve of as-formed nanostructures (sample no. 1 before calcination stage).

the 50 ml of the contaminate solutions and 50 mg of $SrMnO_3$ or $SrMnO_3/Ag$ in the glass reactor was used to determine the photocatalytic process. The mixture of contaminate and catalyst was placed in photoreactor under UV light and stirred for 20 min at dark. The photocatalytic tests were accomplished in a glass vessel with a diameter of 10 cm. A 400W Xe lamp was used as light source. After 10 min, 5 mL of the suspension was sampled and centrifuged. Then, the absorbance spectra of the dyes solution were recorded with a UV-Vis spectrophotometer, and the rate of degradation was observed in terms of change in intensity at λ_{max} of the dyes. The organic contaminant photodegradation efficiency has been determined as follow:

$$Degradation\ (\%) = \frac{C0 - C}{C0} \times 100 \qquad (1)$$

where C and C_0 are the absorbance quantity of organic contaminant solution before and after decomposition by a UV–Vis spectrometer, respectively [25-27].

RESULTS AND DISCUSSION

Thermogravimetry (TG) technique was used to examine of the thermal stability of the as-synthesized nanostructure. Fig. 2 demonstrates the TG curve of the as-prepared powders (sample No. 1 before calcination steps). In this figure,

there are three mass loss stages. The happened endothermic weight loss in the temperature range of 45–250 °C (indicating 4.98 % weight loss) related to the dehydration of the water remaining in the as-synthesized nanostructures. One happened endothermic stage at the temperature range of 250–1000 °C (showing 14.52 % weight loss) may be corresponded to removal of the nitrates and demonstrate the preparation of $SrMnO_3$ nanostructures.

XRD analysis, which is the useful technique for assessment of crystalline structure, was employed to investigate the synthesized $SrMnO_3$ nanostructures. Fig. 3 show the XRD pattern of the $SrMnO_3$ nanostructure prepared with $Mn(NO_3)_2$ and $Sr(NO_3)_2$ precursors. The XRD results for sample 5 before and after calcination are shown in Fig. 3. The presence of (1 0 4), (1 1 0), (1 0 5), (2 0 2), (2 0 3), (1 0 7), (2 1 3), (3 0 0), (1 1 8), (1 0 9) and (2 2 0) peaks in the XRD pattern of SrMnO3 (Fig. 3a) are in accordance with hexagonal structure and JCPDS standard cards no. 24-1221. From the peak of the reflection (1 1 0) of $SrMnO_3$, the particle sizes of the samples was estimated using Sherrer's equation [28-30], $Dc=K\lambda/\beta cos\theta$, Where K is the so-called shape factor, which takes about 0.9, β is the breadth of the observed diffraction line at its half-intensity maximum and λ is the wavelength of X-ray source used in XRD. The average size of the as-obtained nanoparticles was estimated to be 48
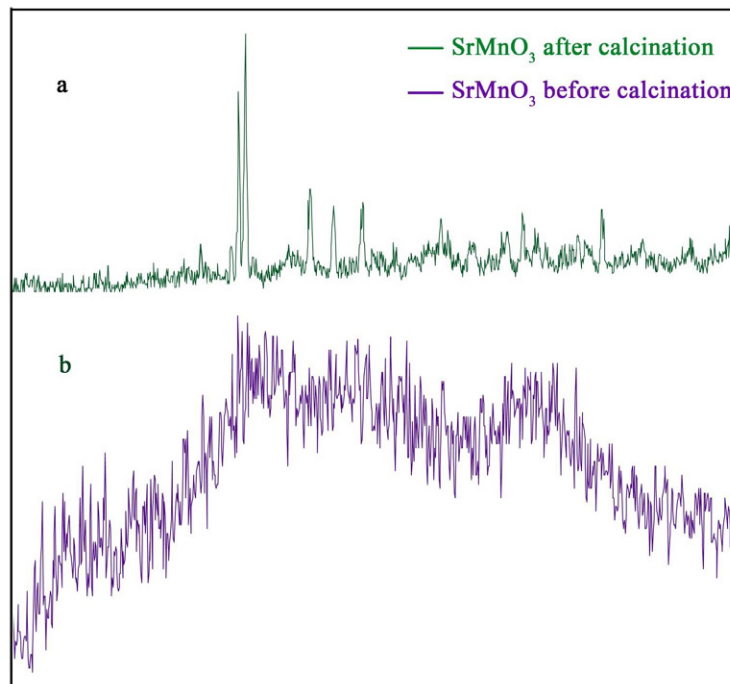
Fig. 3. XRD patterns of (a) SrMnO$_3$ calcinated at 1000 °C and (b) SrMnO$_3$ before calcination
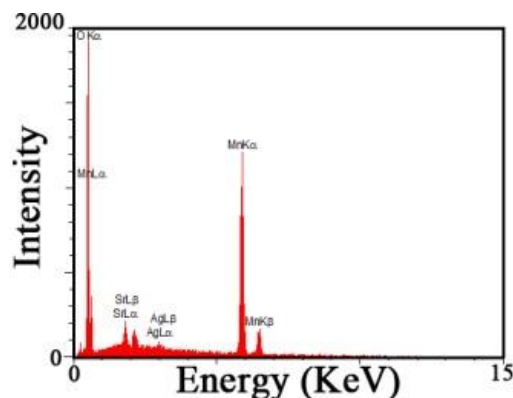

Fig. 4. EDS pattern of SrMnO$_3$/Ag nanostructures

nm. By applying DMG and TEPA as capping agent and alkaline agent, pure SrMnO$_3$ nanostructures have been synthesized (Fig. 3a). As can be seen the crystalline structure and purity of compound is desirable. Fig. 3b demonstrates XRD pattern of sample 4 before calcination, in this case the crystalline structure of SrMnO$_3$ is not desirable.

Then to show Ag in structure, elemental analysis (EDS) analysis was employed. EDX analysis of SrMnO$_3$/Ag nanostructure is showed in Fig. 4. The lines of Sr, Mn, Ag and O are clearly observed and there were no other peaks for impurities.

FT-IR is a rampant analytical that applied to identify organic materials in middle IR region and in some cases inorganic material in far IR region. Fig. 5a shows FT-IR result for synthesized SrMnO$_3$ nanoparticles (sample 5) before calcination. The broad band at 1620 cm^{-1} was assigned to the oxime group in DMG structure. The peak nearly 1384 cm^{-1} is due to stretching vibration of the amine group. The presence of broad band at 3430 cm^{-1} is accordance to the stretching vibrations of surface hydroxyl (–OH) groups. The band at around 841 cm^{-1} is dedicated to the C-H and CH$_2$ vibrations of TETA and DMG.
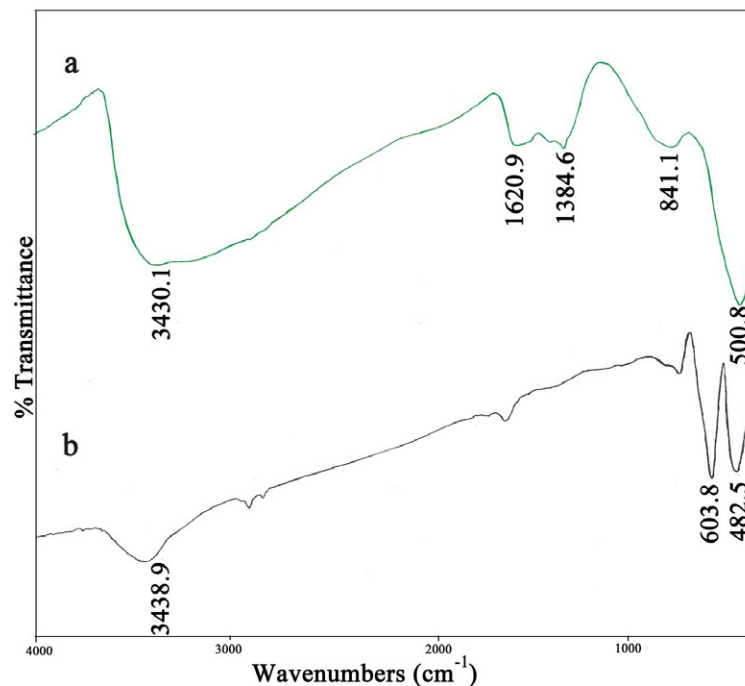
Fig. 5. FT-IR spectra of (a) SrMnO$_3$ nanostructures (sample 5 before calcination) and (b) SrMnO$_3$ nanostructures after calcination (sample 5)

In Fig. 5b two peaks at 482 and 603 cm^{-1} refers to the stretching vibration of the metal-oxygen bond. The presence of these bands indicates that Sr and Mn were situated in an oxygen environment in the hexagonal structure. Also the broad band at 3438 cm^{-1} was assigned to the stretching vibrations of surface hydroxyl (–OH) groups.

The morphologies of nanomaterial were studied by scanning electron microscopy. FESEM technique was used to evaluate the influence of factors such as the kind of capping agent and alkaline agent on the grain size and morphology of the SrMnO$_3$ nanoparticle. To investigate the role of the kind of alkaline agent on the size and morphology of SrMnO$_3$, NH$_3$ and TEPA were utilized (sample Nos. 2, 3). As can be seen in Fig. 6c and d, the synthesized nanoparticles using TEPA as alkaline agent, are more distinctive and less agglomerated in compared with those that prepared using NH$_3$ (Fig. 6a and b). As a result TEPA was chosen as optimum alkaline agent. The TEPA acts as both alkaline agent and capping agent through preventing the aggregation of the prepared nanoparticles. Now by using of TEPA and precursors of Sr and Mn effects of capping agents were investigated. Fig. 7 demonstrates

FESEM images of sample Nos. 4 and 5 prepared in the presence of the 2-hydroxy-1-naphthaldehyde (Fig. 7a and b) and DMG (Fig. 7c and d). Among these the prepared samples, sample No. 4 synthesized by using DMG in presence of TEPA, show homogeneous sphere-like nanoparticles with small particle size. It seems that among were employed capping agent and alkaline agent, DMG and TEPA has the highest steric barrier effect. Furthermore, FESEM images reveals that the increment in the steric barrier effect causes to the grain size of samples becomes small. It seems that the nucleation to be happened rather than the particle growth through increasing the steric barrier effect. Now on the surface of the synthesized nanostructure using TEPA and DMG, which known as the optimum sample, silver nanoparticle was deposited by photodeposition method. Fig. 8a and b depict morphology of SrMnO$_3$/Ag nanocomposite. As can be seen surface and size of SrMnO$_3$/Ag nanostructure (sample 6) is rough and elder in comparison with sample 5 nanostructure, which is evidence for coting of Ag particles on the surface.

Figs. 9a and b demonstrate TEM images of SrMnO$_3$/Ag nanostructures prepared via
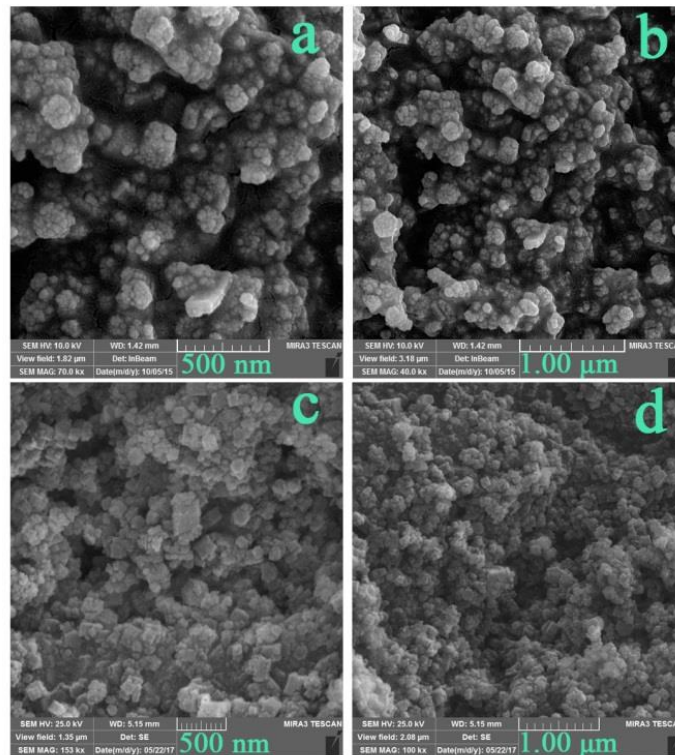
Fig. 6. FESEM images of the samples obtained by various alkaline agents; NH$_3$ (a, b), and TEPA (c, d)
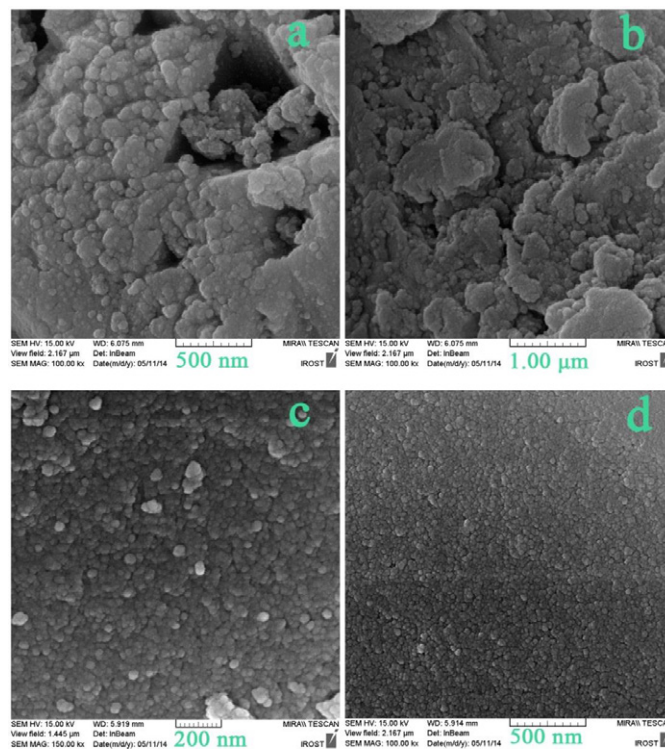

Fig. 7. FESEM images of the products prepared by different capping agents; 2-hydroxy-1-naphthaldehyde (a, b), DMG (c, d)
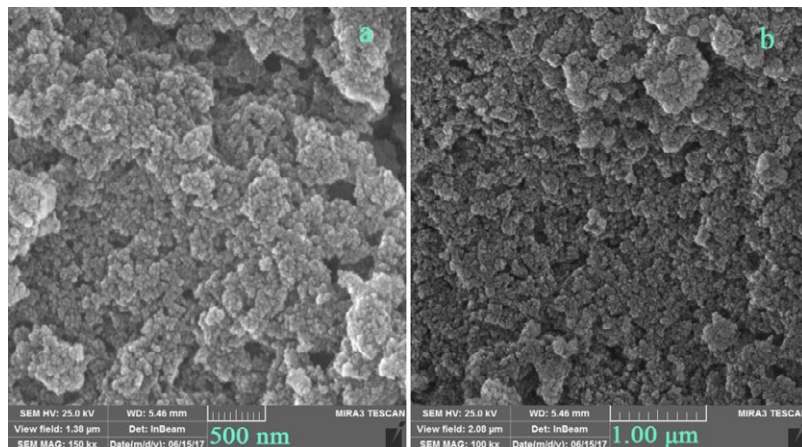
Fig. 8. FESEM images of SrMnO$_3$/Ag nanostructures (sample 6)
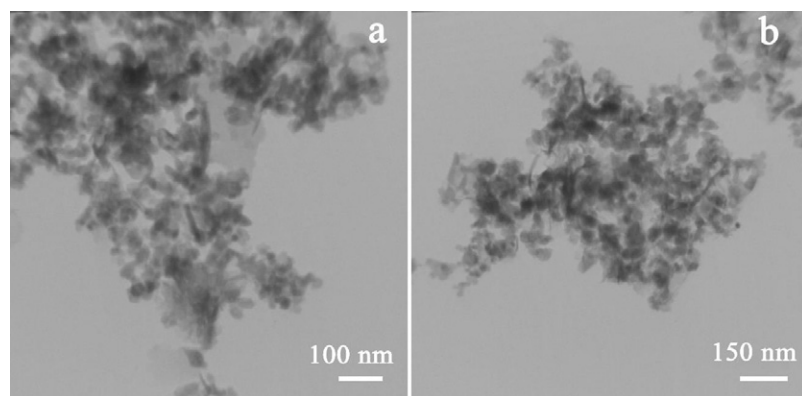
Fig. 9. TEM images of SrMnO$_3$/Ag nanostructures (sample no. 6).

Strontium nitrate and Manganese nitrate and Ag(NO$_3$) precursors in presence of TEPA and DMG as alkaline agent and stabilization agent respectively. The nanostructures with narrow size distribution are clearly seen in TEM images, which are consistent with the above-mentioned SEM analysis (7a, b).

In order to determine the band gap of the SrMnO3 and the SrMnO3/Ag nanostructures, UV–Vis diffuse reflectance analysis was taken. Fig. 10a and b reveals the UV–Vis absorption spectrum of sample No.5 (prepared using TEPA in presence of DMG as capping agent) and 6 (SrMnO$_3$/Ag). The peaks nearly 240, 255, 262, 300, 325, 352, 375 and 392 nm (Fig. 10a) can be seen in the DR-UV-Vis spectrum of sample 5. The band gap can be determined based on the absorption spectrum using Tauc's equation [31, 32]. The band gap value of the nanostructures was obtained through extrapolating the linear

section of the plot of $(\alpha h \nu)^2$ against hν to the energy axis (Fig. 10c). The Eg value of the as-prepared SrMnO$_3$ nanostructures estimated to be 3.22 eV. Fig 10b demonstrates absorption bands at 220, 247, 256, 275, 292, 303, 322, 340,398 and 403 nm for SrMnO$_3$/Ag nanostracure. The Eg of the SrMnO$_3$/Ag nanostructure (sample no. 6) estimated to be around 3.1 eV (Fig. 10d). From the calculated Eg value, as-prepared SrMnO$_3$/Ag and SrMnO$_3$ samples may be employed as the photocatalyst under UV illustration.

The role of various stabilization agents and alkaline agent on the photocatalytic efficiency of SrMnO$_3$ has been investigated through monitoring the destruction of various dyes pollutant under ultraviolet illumination. The influence of various factors including kind of pollutant, grain size and morphology of SrMnO$_3$ nanoparticles, pH and amount of photocatalyst on photocatalytic activity of products were examined. Reaction model of
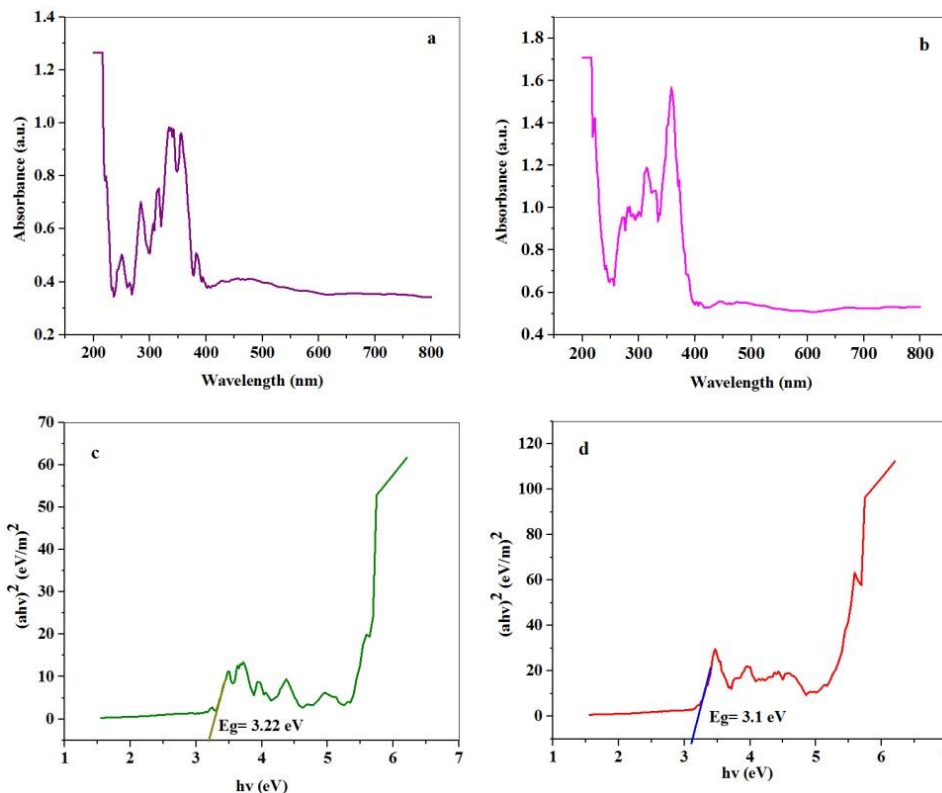
Fig. 10. UV–Vis diffuse reflectance spectrum and plot to determine the band gap of the SrMnO$_3$ (sample5) (a and c) and UV–Vis diffuse reflectance spectrum and plot to determine the band gap of the SrMnO$_3$/Ag nanostructures (sample 6) (b and d)

the SrMnO$_3$/Ag nanostructure for photocatalytic activity is proposed as shown in Fig. 11.

Also the offered mechanism of the decomposition of dyes can be summarized as:

$SrMnO_3/Ag + hv \rightarrow SrMnO_3/Ag^* + e^- + h^+$

$h^+ + H_2O \rightarrow OH^. + H^+$

$2e^- + O_2 + 2H^+ \rightarrow O_2^{.-}$

$OH^. + O_2^{.-} + Pollutants \rightarrow Destruction products$

During the photocatalytic process, the generated electron and holes may migrate to the catalyst surface where they participate in redox reactions with adsorbed species. The h$^+$ may interact with H$_2$O to product the hydroxyl radical (OH$^.$). Also e$^-$ may interact with O$_2$ to produce the oxygen radical (O$_2^{.-}$). It has been suggested that the hydroxyl radicals (OH$^.$) and oxygen radical (O$_2^{.-}$) are the essential oxidizing species in the photocatalytic perocess. For blank sample no dye degradation was observed after 70 min without using UV light irradiation or photocatalyst. In the base of this observation, the contribution of self-degradation is insignificant.

Fig. 11. Schematic diagram of the reaction mechanism of rhodamine B photodegradation by SrMnO$_3$/Ag

The photocatalytic activity of samples 4, 5 and 6 was evaluated for demolition of rhodamine B, the results are shown in Fig. 12. As it can be seen photocatalyst performance of sample 6 (SrMnO$_3$/Ag nanostructure) is much higher than that of samples 4 and 5. From the photocatalytic calculations, the rhodamine B contaminate destruction were about 54% by sample 4, about
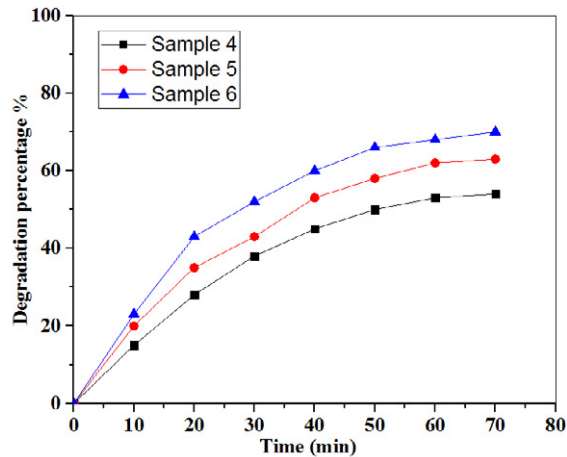
Fig. 12. The photocatalytic behavior of the as-prepared nanostructures (samples 4, 5 and 6)
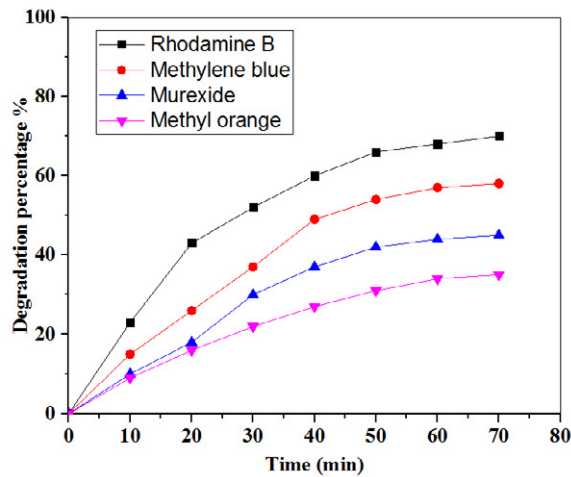
Fig. 13. The photocatalytic behavior of SrMnO$_3$/Ag nanostructures (sample 6) on decomposition of rhodamine B, methyl orange, methylene blue and murexide

63% sample 5 and about 70% by sample 6 after 70 min UV irradiation. By comparing the SEM images of as-prepared nanostructures (Figs. 7a-d) it can be observed that the use of TEPA and DMG (sample 5) is satisfactory for the production of uniform spherical SrMnO$_3$ nanostructure. Because whatever the particle size is smaller the ratio of surface area to volume increases, therefore the catalytic performance is better. The photocatalytic activity of sample 6 (SrMnO$_3$/Ag) is better than other samples, because of two reasons; first, Ag particles were selectively deposited on the electron trapping sites in photodeposition process, so the resulting Ag particles will serve as new electron sumps to entrap electron and extract of them to demolition of dye. Second, it

is generally admitted that the recombination of electron (e$^-$) and hole (h$^+$) has a significant impact on the photocatalytic performance. By decreasing the recombination of electron (e$^-$) and hole (h$^+$), the photocatalysis activity is increased. When the band gap decreases, the chance of recombination of electron (e$^-$) and hole (h$^+$) can be decreased, whereupon photocatalysis activity increases. In the case of nanostructured SrMnO$_3$/Ag with lower energy gap quantity then SrMnO$_3$, the electron and hole recombination is reduced and therefore the better photocatalytic performance is observed [33]. In the next step, the photocatalytic performance of SrMnO$_3$/Ag was investigated for decomposition of MO, murexide and MB, and the results were shown in Fig. 13. The catalysis
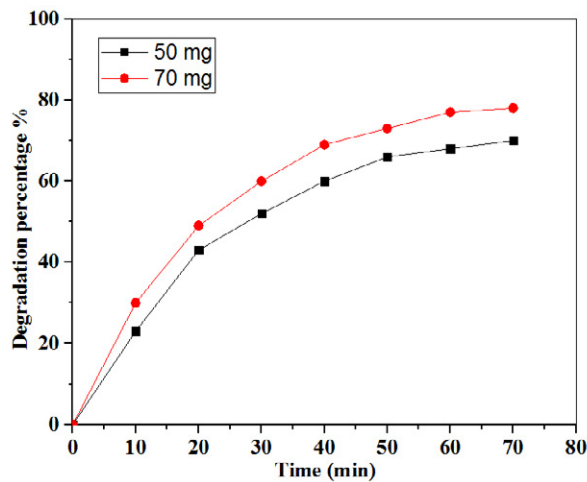
Fig 14. The influence of the concentration of photocatalyst (sample 6) on the photocatalytic performance for degradation of rhodamine B
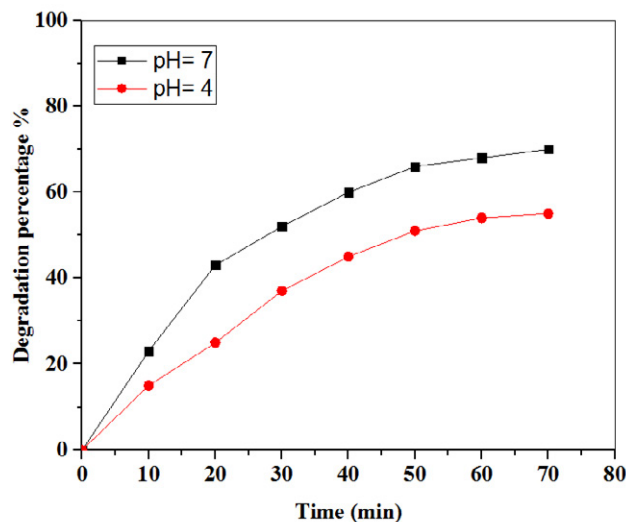
Fig. 15. Effect of pH on the photocatalytic decomposition of rhodamine B

efficiency of methyl orange, murexide and methylene blue are 35%, 45% and 58% respectively. It is evident that the photocatalytic destruction of anionic contaminants with a negative charge is weaker than cationic contaminants with a positive charge. The greatest amount of photocatalytic decomposition is for rhodamine B. These results reveal that in photocatalytic process, the cationic pollutant adsorption on the $SrMnO_3$/Ag is better than of adsorption of anionic contaminant on it. Forasmuch as the nanostructured $SrMnO_3$/Ag has oxygen atoms with a great electron density on its surface, it seems that $SrMnO_3$/Ag with negative charge can adsorb the cationic pollutant with positive charge. Fig. 14 reveals the effect of various

amount of photocatalyst on the photocatalytic performance of $SrMnO_3$/Ag nanostructure. It can be seen that dye removal efficiency increased with the increase of photocatalyst concentration. The results illustrate that the percentage decomposition of rhodamine B under UV light increased from 70% to 78% with changing amount of photocatalyst from 50 to 70 mg in 50 ml of the contaminate solutions. The pH of the solution is known as effective parameter in the photocatalytic reactions. For investigate of the pH role on the destruction rate, two values of pH were tested. Destruction of rhodamine B was measured under acidic (pH=4) and neutral conditions (pH= 7) (Fig. 15). From photocatalytic calculations, the

Fig. 16. Effect of pH on the adsorption and desorption rhodamine B on the surface of SrMnO$_3$/Ag nanostructures

rhodamine B pollutant degradation was about 55% at pH= 5 and 70% at pH= 7 after 70 min UV illustration. By reducing pH, absorption of rhodamine B on the surface of the nanocatalyst is reduced. As shown in Fig. 16, in acidic and basic conditions the surface of nanostructures is covered by more positive and negative charge respectively. In acidic condition cationic molecules can be more desorbed on the surface. Subsequently, it can be seen that maximum demolition for rhodamine B was obtained in the neutral condition.

CONCLUSION

In this work, SrMnO$_3$ nanostructures were prepared by co-precipitation method. The effect capping agent, alkaline agent and calcination temperature were investigated on size and morphology of product. Results show that the best product has been achieved in presence of TEPA and DMG. In the next step, silver particle deposited on this pure nanoparticle. Results show that preparation conditions have been influenced on size and morphology of nanostructures and have the most important effect on the photocatalytic performance. The influences of various factors including kind of pollutant, grain size of SrMnO$_3$ nanostructures, amount of SrMnO$_3$/Ag and pH on photocatalytic activity of products were evaluated. It was observed that by using of SrMnO$_3$/Ag nanostructure instead SrMnO$_3$ nanoparticles the photocatalytic performance increased. Also results suggest that SrMnO$_3$/Ag nanoparticles are interesting and desirable candidate for photocatalytic applications under UV light.

CONFLICT OF INTEREST

The authors declare that there is no conflict of interests regarding the publication of this manuscript.

REFERENCES

1. Pan JH, Dou H, Xiong Z, Xu C, Ma J, Zhao XS. Porous photocatalysts for advanced water purifications. Journal of Materials Chemistry. 2010;20(22):4512.
2. Seo HO, Sim CW, Kim K-D, Kim YD, Lim DC. Nanoporous TiO2/SiO2 prepared by atomic layer deposition as adsorbents of methylene blue in aqueous solutions. Chemical Engineering Journal. 2012;183:381-6.
3. Dutta S, Parsons SA, Bhattacharjee C, Jarvis P, Datta S, Bandyopadhyay S. Kinetic study of adsorption and photo-decolorization of Reactive Red 198 on TiO2 surface. Chemical Engineering Journal. 2009;155(3):674-9.
4. Xiong Z, Ma J, Ng WJ, Waite TD, Zhao XS. Silver-modified mesoporous TiO2 photocatalyst for water purification. Water Research. 2011;45(5):2095-103.
5. Han F, Kambala VSR, Srinivasan M, Rajarathnam D, Naidu R. Tailored titanium dioxide photocatalysts for the degradation of organic dyes in wastewater treatment: A review. Applied Catalysis A: General. 2009;359(1-2):25-40.
6. Jagadeesan D, Mansoori U, Mandal P, Sundaresan A, Eswaramoorthy M. Hollow Spheres to Nanocups: Tuning the Morphology and Magnetic Properties of Single-Crystalline α-Fe2O3Nanostructures. Angewandte Chemie. 2008;120(40):7799-802.
7. Chhabra V, Ayyub P, Chattopadhyay S, Maitra AN. Preparation of acicular γ-Fe2O3 particles from a microemulsion-mediated reaction. Materials Letters. 1996;26(1-2):21-6.
8. Janot R, Guérard D. One-step synthesis of maghemite nanometric powders by ball-milling. Journal of Alloys and Compounds. 2002;333(1-2):302-7.

9. Bee A, Massart R, Neveu S. Synthesis of very fine maghemite particles. Journal of Magnetism and Magnetic Materials. 1995;149(1-2):6-9.

10. Melo Jorge ME, Nunes MR, Silva Maria R, Sousa D. Metal–Insulator Transition Induced by Ce Doping in CaMnO3. Chemistry of Materials. 2005;17(8):2069-75.

11. Sousa D, Nunes MR, Silveira C, Matos I, Lopes AB, Melo Jorge ME. Ca-site substitution induced a metal–insulator transition in manganite CaMnO3. Materials Chemistry and Physics. 2008;109(2-3):311-9.

12. Isasi PH, Lopes ME, Nunes MR, Melo Jorge ME. Low-temperature synthesis of nanocrystalline Ca1−xHoxMnO3−δ (0⩽x⩽0.3) powders. Journal of Physics and Chemistry of Solids. 2009;70(2):405-11.

13. Haghiri-Gosnet AM, Renard JP. CMR manganites: physics, thin films and devices. Journal of Physics D: Applied Physics. 2003;36(8):R127-R50.

14. Fisher B, Patlagan L, Reisner GM, Knizhnik A. Systematics in the thermopower of electron-doped layered manganites. Physical Review B. 2000;61(1):470-5.

15. Cohn JL, Neumeier JJ. Heat conduction and magnetic phase behavior in electron-dopedCa1−xLaxMnO3(0<~x<~0.2). Physical Review B. 2002;66(10).

16. Zeng Z, Greenblatt M, Croft M. Charge ordering and magnetoresistance ofCa1−xCexMnO3. Physical Review B. 2001;63(22).

17. Sacchetti A, Baldini M, Crispoldi F, Postorino P, Dore P, Nucara A, et al. Temperature dependence of the optical phonons inSrMnO3manganite: Evidence of a low-temperature structural transition in the hexagonal compound. Physical Review B. 2005;72(17).

18. Lee KJ, Iguchi E. Electronic Properties of SrMnO3-x. Journal of Solid State Chemistry. 1995;114(1):242-8.

19. Heiras J, Pichardo E, Mahmood A, López T, Pérez-Salas R, Siqueiros JM, et al. Thermochromism in (Ba,Sr)-Mn oxides. Journal of Physics and Chemistry of Solids. 2002;63(4):591-5.

20. Duprat AM, Alphonse P, Sarda C, Rousset A, Gillot B. Non-stoichiometry-activity relationship in perovskite-like manganites. Materials Chemistry and Physics. 1994;37(1):76-81.

21. Taguchi H, Matsuda D, Nagao M, Tanihata K, Miyamoto Y. Synthesis of Perovskite-Type (La1−xSrx)MnO3(OX0.3) at Low Temperature. Journal of the American Ceramic Society. 1992;75(1):201-2.

22. Shimizu Y, Murata T. Sol-Gel Synthesis of Perovskite-Type Lanthanum Manganite Thin Films and Fine Powders Using Metal Acetylacetonate and Poly(vinyl alcohol). Journal of the American Ceramic Society. 2005;80(10):2702-4.

23. Khazaei M, Malekzadeh A, Amini F, Mortazavi Y, Khodadadi A. Effect of citric acid concentration as emulsifier on perovskite phase formation of nano-sized SrMnO3 and SrCoO3 samples. Crystal Research and Technology. 2010;45(10):1064-8.

24. Yuh J, Perez L, Sigmund WM, Nino JC. Sol-gel based synthesis of complex oxide nanofibers. Journal of Sol-Gel Science and Technology. 2007;42(3):323-9.

25. Fauzian M, Taufik A, Saleh R. Improvement of catalytic activity of Fe3O4/CuO/TiO2 nanocomposites using the combination of ultrasonic and UV light irradiation for degradation of organic dyes. Author(s); 2016.

26. Abbasi A, Khojasteh H, Hamadanian M, Salavati-Niasari M. Synthesis of CoFe2O4 nanoparticles and investigation of the temperature, surfactant, capping agent and time effects on the size and magnetic properties. Journal of Materials Science: Materials in Electronics. 2016;27(5):4972-80.

27. Ghanbari M, Gholamrezaei S, Salavati-Niasari M, Abbasi A. Synthesis and characterization of Ag2CdI4 nanoparticles and photo-degradation of organic dyes. Journal of Materials Science: Materials in Electronics. 2017;28(8):6272-7.

28. Abbasi A, Ghanbari D, Salavati-Niasari M, Hamadanian M. Photo-degradation of methylene blue: photocatalyst and magnetic investigation of Fe2O3–TiO2 nanoparticles and nanocomposites. Journal of Materials Science: Materials in Electronics. 2016;27(5):4800-9.

29. Khojasteh H, Salavati-Niasari M, Abbasi A, Azizi F, Enhessari M. Synthesis, characterization and photocatalytic activity of PdO/TiO2 and Pd/TiO2 nanocomposites. Journal of Materials Science: Materials in Electronics. 2015;27(2):1261-9.

30. Mortazavi-Derazkola S, Salavati-Niasari M, Amiri O, Abbasi A. Fabrication and characterization of Fe 3 O 4 @SiO 2 @ TiO 2 @Ho nanostructures as a novel and highly efficient photocatalyst for degradation of organic pollution. Journal of Energy Chemistry. 2017;26(1):17-23.

31. Abbasi A, Hamadanian M, Salavati-Niasari M, Mazhari MP. Hydrothermal synthesis, characterization and photodegradation of organic pollutants of CoCr2O4/Ag nanostructure and thermal stability of epoxy acrylate nanocomposite. Advanced Powder Technology. 2017;28(10):2756-65.

32. Abbasi A, Hamadanian M, Salavati-Niasari M, Mortazavi-Derazkola S. Facile size-controlled preparation of highly photocatalytically active ZnCr2O4 and ZnCr2O4/Ag nanostructures for removal of organic contaminants. Journal of Colloid and Interface Science. 2017;500:276-84.

33. Abbasi A, Khojasteh H, Hamadanian M, Salavati-Niasari M. Normal spinel CdCr2O4 and CdCr2O4/Ag nanocomposite as novel photocatalysts, for degradation of water contaminates. Separation and Purification Technology. 2018;195:37-49.